Biomaterials Science

ROYAL SOCIETY OF CHEMISTRY

PAPER

View Article Online
View Journal | View Issue

Cite this: *Biomater. Sci.*, 2023, **11**, 583

Intradermal delivery of an angiotensin II receptor blocker using a personalized microneedle patch for treatment of hypertrophic scars†

Yihui Huang,‡[a] Jingwen Li,‡[b] Yan Wang,[b] Danyang Chen,[a] Jianglong Huang,[c] Wubin Dai,[d] Pan Peng,[a] Liang Guo*[a] and Yifeng Lei *[b]

High-quality postoperative rehabilitation is the focus of most patients currently, and hypertrophic scar (HS) greatly reduces the patient's quality of life due to the symptom of severe itching. Traditional HS therapies are associated with limitations, such as poor drug delivery efficiency for topical administration and severe pain for intralesional injection. In this study, we developed a personalized microneedle patch system for minimally invasive and effective treatment of HSs. The microneedle patches were personalized designed and fabricated with 3D printing in order to adapt to individual HS. The optimized microneedle patches were composed of dissolving gelatin and starch and loaded with losartan. Losartan, as a drug class of angiotensin II receptor blockers (ARBs), can effectively inhibit the proliferation and migration of hypertrophic scar fibroblasts (HSFs) and downregulate the gene expression related to scar formation in HSFs. The dissolving microneedle patches exhibited strong mechanical strength, effectively penetrated the stratum corneum of HSs and increased the losartan delivery into HSs upon dissolution of gelatin and starch. Together, the losartan-loaded microneedle patches effectively inhibited the formation of HSs in rabbit ears with reduced scar elevation index (SEI), and decreased fibrosis and collagen deposition in HSs. This personalized microneedle patch system increases the drug delivery efficiency into HSs with minimal invasion, and opens a new window for personalized management and treatment of skin diseases.

Received 7th October 2022,
Accepted 23rd November 2022

DOI: 10.1039/d2bm01631a

rsc.li/biomaterials-science

1. Introduction

In the past decades, the mortality of major trauma has been significantly reduced and high-quality postoperative rehabilitation is currently the focus of most patients. Hypertrophic scar (HS) is a thickened and raised scar resulting from an abnormal response during wound healing of trauma or injury,[1] where fibroblasts proliferate and excessive collagen deposits in the dermis.[2] Although HS may finally stabilize or gradually regress, the symptom of severe itching greatly reduces the patient's quality of life.[3] Effective HS treatments relieve patients from discomfort and satisfy their aesthetic demands.

Currently, common treatments for HS include surgery, topical drug administration, compression therapy, radiation, and laser treatment.[4,5] However, these treatments are associated with some limitations, such as high recurrence rate after surgery, poor effect of compression therapy, serious side effects of radiotherapy, and repeated treatment required during laser therapy. Due to hyperplasia and dysfunction of the stratum corneum of HSs, topical drug administration on HSs shows a poor drug delivery efficiency. Moreover, intralesional injection is used in the treatment of HSs. However, with excessive deposition of collagen in the dermis, the HS tissue is dense and hard, and therefore the tension in the scar significantly increases upon injection, which causes severe pain even with local anesthetics. In addition, the effect of injection for HS treatment strongly depends on the skill of operators and an improper injection may lead to poor treatment effects and even the occurrence of side effects.[1] Therefore, it is necessary to develop more efficient drug delivery strategies with better therapeutic effects for HS treatment.

Microneedles (MNs) represent a novel technology for drug delivery.[6–8] With micrometer-scaled needles arranged in a designed patch, the microneedle patch system has advantages such as minimal invasion and personalized and precise drug release and has attracted emerging attention in biosensing,[9,10]

[a]*Department of Plastic Surgery, Zhongnan Hospital of Wuhan University, Wuhan 430071, China. E-mail: guolianghbwh@163.com*
[b]*The Institute of Technological Science & School of Power and Mechanical Engineering, Wuhan University, Wuhan 430072, China. E-mail: yifenglei@whu.edu.cn*
[c]*Department of Dermatology and Cosmetic Medicine, Hubei Aerospace Hospital, Xiaogan 432000, China*
[d]*School of Material Science and Engineering, Wuhan Institute of Technology, Wuhan 430205, China*

†Electronic supplementary information (ESI) available. See DOI: https://doi.org/10.1039/d2bm01631a

‡These authors contributed equally to this work.

diagnosis,[11] and treatments of different diseases including diabetes,[12–14] cancers,[15,16] wounds,[17–19] scars,[20–22] and psoriasis.[23] The stratum corneum is the main barrier of the skin and limits the efficiency of transdermal drug penetration.[24] With drugs loaded in the microneedle patches, the drugs can pass through the stratum corneum and be delivered into the dermis through the skin-breaking effect of microneedles, which significantly improve the drug delivery efficiency.[24]

Different drugs were administrated for HS therapy clinically, among which glucocorticoids (such as triamcinolone acetonide and betamethasone) and antineoplastic drugs (such as 5-fluorouracil) are most commonly used.[25] However, repeated application of glucocorticoids may lead to vasodilation and menstrual disorders in female patients.[26] Local application of antineoplastic drugs on HSs has a risk of bone marrow suppression or adverse gastrointestinal reactions, and patients need regular blood tests to avoid serious side effects.[4] Otherwise, the renin–angiotensin system (RAS) is highly associated with the formation of HSs,[27] including angiotensin II, angiotensin-converting enzyme (ACE), which converts angiotensin I to angiotensin II, angiotensin II receptor type 1 (AT1 receptor) and type 2 (AT2 receptor).[27,28] For instance, ACE was over expressed in human scar fibroblasts (HSFs), and the activity of ACE enhanced in scar tissues,[29] and angiotensin II promoted collagen deposition in HSs.[30] Moreover, AT1 receptor is one of the key players in the formation of HSs, which contributed to cell proliferation and migration, fibrosis, and inflammation.[27] Therefore, the administration of angiotensin II receptor blockers (ARBs) has great potential for treatment of HSs. Among ARBs, losartan is a representative blocker of the AT1 receptor, with high affinity, specificity and competitiveness to the AT1 receptor.[31]

Taking the above points into consideration, herein in this study, we aim to establish a personalized dissolving microneedle array patch loaded with losartan, and investigate its effect on the treatment of HSs in rabbit ears. We found that losartan, as a drug class of ARBs, effectively inhibited the viability and migration of human HSFs, and down-regulated the gene expression relative to scar formation in HSFs. The personalized microneedle patches enhanced the penetration and losartan delivery into the dermis of HSs, and effectively inhibited the formation of HSs in rabbit ear with inhibited fibrosis and decreased collagen deposition.

2. Materials and methods

2.1. Materials

All materials used in the experiment were purchased directly without further purification. Gelatin, starch and hydroxyapatite nanoparticles were purchased from Sigma-Aldrich, Shanghai, China. Losartan and rhodamine 6G were purchased from Aladdin, Shanghai, China. Polydimethylsiloxane (PDMS) reagents were obtained from DowCorning, Shanghai, China. Ultrapure water (Milli-Q) with a resistivity of 18.2 M was used throughout the study.

2.2. Cell culture

Human HSFs were isolated from human HS tissues according to our previous study,[32] under ethical approval of the Ethics Committees of Zhongnan Hospital of Wuhan University (Approval No. 2021115), and informed consent was obtained from patients for use of HS tissues.

The isolated HSFs were cultured in a standard cell culture medium of DMEM/F-12 medium (Gibco™) supplemented with 10% fetal bovine serum (FBS, VivaCell™) and 1% penicillin and streptomycin (PS, Biosharp™). The cells were incubated in a humidified incubator at 37 °C, with 5% CO_2 and 95% relative humidity. HSFs were passed every 4–5 days to maintain a logarithmic growth.

2.2.1. Cell viability test. CCK-8 assay was carried out to evaluate the cytotoxicity of losartan on HSFs. In brief, HSFs were plated on 96-well plates (1×10^4 per well) for 24 h, and then incubated with cell culture medium with different concentrations of losartan (1, 10, 100, and 1000 μM) or with standard cell culture medium as the control. After incubation for 24 h, cells were washed and treated with CCK-8 (Dojindo Laboratories™, 10 μL for each well) for 2 h. Then the absorbance of the plate was measured using a microplate reader (Thermo Fisher Scientific) at 450 nm. Cell viability was calculated according to the absorbance of different groups. Each treatment was conducted at least in triplicate.

2.2.2. Cell migration assay. The influence of losartan on migration of HSFs was evaluated using scratch assay. Briefly, HSFs were seeded in a six-well plate (1×10^5 per well), and incubated with standard cell culture medium until 90% confluence. Subsequently, sterile pipette tips were used to make a scratch in the middle of the adherent cells in each well. Cells were washed and further incubated with the control medium or medium with different concentrations of losartan (1, 10, and 100 μM). After further incubation for 24 h, the samples were observed under bright-field microscopy (Olympus BX51). The wound gaps were measured and the percentage of scratch closure was calculated using ImageJ software (National Institutes of Health, Version 1.48). Each treatment was quantified in triplicate.

2.2.3. RT-PCR assay. RT-PCR was conducted to investigate the impact of losartan on the gene expression of HSFs related to scar formation. In brief, HSFs were plated on 96-well plates (1×10^4 per well) and incubated with different media for 24 h. Then total RNA was harvested from the collected cells using TRIzol reagent (Invitrogen™), and the concentration of total RNA was quantified under an ultramicro spectrophotometer (NanoDrop™ one, Thermo Fisher Scientific). A HiScript III RT SuperMix reverse transcription kit (Vazyme Biotech, China) was used to generate the reverse transcription and RNA was reversely transcribed into cDNA. Real-time PCR was performed using ChamQ SYBR qPCR Master Mix in a 7500 Real-Time PCR system (Applied Biosystems), and equal amounts of cDNA were added during the procedure. The following primer sequences were used for amplification (Table 1), including transforming growth factor-β1 (TGF-β1), collagen I, interleu-

Table 1 Primers used for RT-PCR assay in HSFs

Primer name	Function	Sequence
TGF-β1	Forward	GGAAATTGAGGGCTTTCGCC
	Reverse	CCGGTAGTGAACCCGTTGAT
Collagen I	Forward	GAGGGCCAAGACGAAGACATC
	Reverse	CAGATCACGTCATCGCACAAC
IL-6	Forward	ACTCACCTCTTCAGAACGAATTG
	Reverse	CCATCTTTGGAAGGTTCAGGTTG
Smad3	Forward	GCGCACTGACCATAAGAGCA
	Reverse	ATCCAGGGACTCAAACGTGG

kin-6 (IL-6), and small mother against decapentaplegic 3 (Smad3). The fold induction was analyzed using the $2^{-\Delta\Delta CT}$ relative quantification technique. Each treatment was conducted in triplicate.

2.3. Fabrication and characterization of microneedle patches

2.3.1. Design and 3D printing of personalized master molds. In order to adapt to the HSs with different shapes and different thicknesses (Fig. 1A, insets), we used a stereolithographic 3D printer (Form 3, USA) to print different master molds (Fig. S1†). In brief, three-dimensional molds in resin were personalized designed using Solidworks software, and uploaded into the 3D printer for printing (Fig. S1A†). Then, PDMS solution containing 10% crosslinking agent was poured onto the resin mold and cured at 90 °C for 30 min, and then the resin mold was removed to obtain the personalized PDMS mold (Fig. 1A and Fig. S1B†).

2.3.2. Fabrication of microneedle patches. Gelatin and starch were selected as the basic materials for preparation of microneedle patches. First, three different compositions were used for optimization of materials (Table 2 and Table S1†) based on our previous studies.[13,14] Further, the optimized material composition was used to prepare the microneedle patches loaded with different concentrations of losartan (Table 3), by using the above prepared personalized PDMS molds (Fig. 1A and Fig. S1†). Briefly, the gelatin-starch mixture with different concentrations of losartan was poured on the surface of the PDMS mold, and centrifuged at 3500 rpm for 20 min. The process was repeated three times to fill the cavity

Table 2 Different material compositions of microneedle patches

Name	Gelatin (m/v)	Starch (m/v)	Hydroxyapatite (m/v)
M1	5%	5%	0
M2	10%	5%	0

Table 3 Microneedle patches loaded with different concentrations of losartan

Name	Losartan concentration (mg mL^{-1})
LMN-1	50
LMN-2	5
LMN-3	0.5
LMN-4	0.05

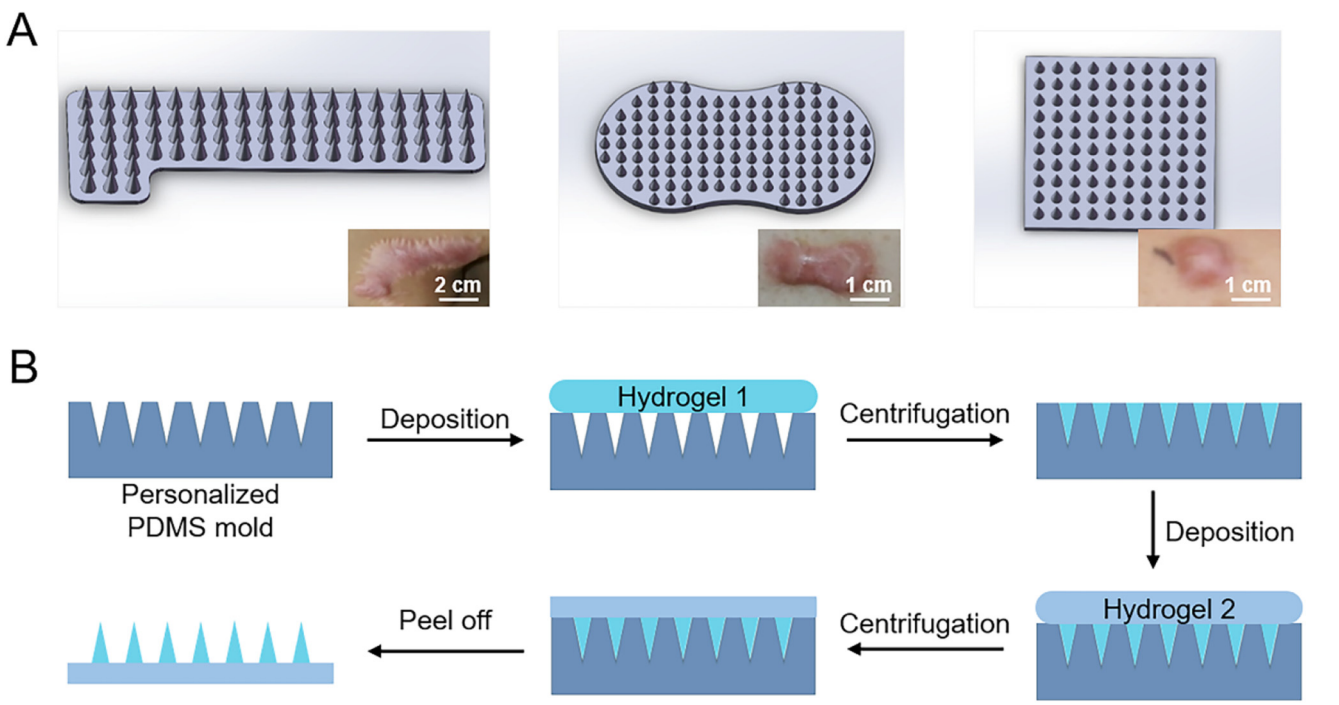

Fig. 1 Schematic design and fabrication of microneedle patches. (A) Personalized design of microneedle patches, which correspond to different shapes of HSs. The insets are images of human HSs with different shapes. (B) Schematic fabrication process of microneedle patches.

of the mold (Fig. 1B). Then, the microneedle substrate was prepared with a similar process. After drying at room temperature for 12 h, the microneedle patch was gently peeled off from the PDMS mold for experiments (Fig. 1B). Moreover, a fluorescent marker of rhodamine 6G can be loaded into the microneedle patch for better visualization.

2.3.3. Characterization of microneedle patches. The morphology of the prepared microneedle patches was visualized with a high-resolution mobile phone (Huawei Mate 40 Pro) and scanning electron microscopy (SEM, TESCAN MIRA3, Czech).

The mechanical properties of microneedle patches composed of different material compositions were measured and compared using a universal testing machine (UTM2503, Suns Technology, China). In compression mode, the feed speed of the compression probe was set at 0.01 mm min^{-1}, and the feed distance was 900 μm to ensure the microneedles being completely crushed. The force-displacement curves during the compression were recorded, and the mechanical properties of the microneedle patches were analyzed and compared.

2.3.4. *In vitro* drug release from microneedles. To evaluate the drug release behavior *in vitro*, microneedles were scraped off from the rhodamine 6G-loaded microneedle patches. Same weights of microneedles were immersed into 1 mL PBS at 37 °C (n = 3 for each group). At different time points, 200 μL solution was collected and transferred into a 96-well plate. The absorbance of the released rhodamine 6G was measured using a microplate reader at 530 nm (Thermo Fisher Scientific). Then drug release was normalized according to the maximum concentration of the released drugs.

2.3.5. Insertion assay of the microneedle patch in porcine skin. To further evaluate the mechanical property of the microneedle patches, the microneedle patches pre-loaded with rhodamine 6G were inserted into fresh porcine skin for 10 min. Then the inserted porcine skin was fixed in 4% paraformaldehyde for 18 h. The samples were embedded by O.C.T compound (SAKURA Tissue-Tek®, USA), and sectioned into 10 μm-slices perpendicular to the skin surface using a microtome (Leica RM 2245, Germany). Subsequently, the sections were visualized using a fluorescence microscope (Olympus, IX73) at 543 nm excitation and 560 nm emission, to investigate the distribution of rhodamine 6G in the cross-sections of the pierced porcine skin.

2.4. Animal study

2.4.1. Animals. All procedures of animal study were approved by the Animal Ethical and Welfare Committee of Zhongnan Hospital of Wuhan University (Approval No. ZN2021199) and were performed in accordance with the National Institutes of Health guidelines for the care and use of laboratory animals.

New Zealand rabbits weighing approximately 2.5–3.0 kg were obtained from the Institute of Laboratory Animal Center, Hubei, China, and raised in Hubei Provincial Center for Safety Evaluation of Food and Drug.

2.4.2. Establishment of the rabbit HS model. The HS model was established in New Zealand rabbits based on previously published protocols.[33,34] Briefly, the rabbits were weighed, and anesthetized by ear vein injection of 1% pentobarbital (3 mL kg^{-1}). The target areas in the ventral side of rabbit ear were sterilized, and full-thickness skin was resected, and then the perichondrium under the skin was completely removed. Four 1 cm × 1 cm wounds were created in each ear. Then the wounds were cleaned using saline and were dressed with gauze (Winner Medica, China). The wounds were daily inspected. After 7 days, rabbits were anaesthetized again, and the scabs formed at the wound sites were gently removed in order to accelerate the formation of scars. After another 7 days, the scabs appeared again at the wound sites, which would naturally fall off from the wound sites within a few days. At 21 days post resection, the resulting wound areas showed typical features of red color and protruded surface, indicating the successful establishment of the HS model.[33,34] The total time for establishment of the HS model was 21 days.

2.4.3. Insertion assay of the microneedle patch in rabbit HSs. HS tissues were collected from the rabbit ear, in order to further assess the penetration ability of losartan-loaded MNs into HSs, including LMN-1, LMN-2, LMN-3 and LMN-4, respectively. As described above, the losartan-loaded MNs were pierced into HS tissues for 5 min by thumb pressing. Then the HS tissues were fixed in 4% paraformaldehyde, embedded with paraffin and sectioned. The samples were subjected to hematoxylin and eosin (H&E) staining and visualized under a bright-field microscope (Olympus BX51). The microchannels formed in the HS tissues were photographed and the depth of microchannels was measured accordingly using ImageJ.

Meanwhile, the dissolution of losartan-loaded MNs upon interaction with rabbit HSs was also investigated. Briefly, the MNs were penetrated into the rabbit HSs by thumb pressing for 1 min. Subsequently, the MNs were fixed on the HSs with a medical tape for another 10 min. Afterwards, the MNs were removed from HSs, and visualized under a high-resolution mobile phone and SEM.

2.4.4. Treatment effect of rabbit HSs with microneedle patches. The treatment effect of losartan-loaded MNs on the above rabbit HSs was investigated. The rabbit HSs were divided into different treatment groups, including drug-free MN, losartan-loaded MN (LMN-1, LMN-2, LMN-3 and LMN-4), losartan cream with the same dosage as LMN-4, and commercialized Mepiform® soft silicone sheeting (Molnlycke Health Care, Sweden). HSs without treatment served as the control group. Each group contained 5 rabbit HSs. For the drug-free MN and losartan-loaded MN groups, one patch was inserted into one HS site by thumb pressing for 1 min, and fixed on the site with a medical tape for 10 min. For losartan cream treatment, the cream was evenly applied onto the surface of HSs. For the Mepiform group, one piece of Mepiform (1.5 cm × 1.5 cm) was adhered on the HS area.

All groups received three administrations on Day 1, Day 8, and Day 15 after creation of the HS model, respectively. Photos of HSs were captured before administration and at one-week

post each administration. Afterwards, the HS tissues were collected for histological analysis as described above, including H&E staining and Masson's trichrome staining, and the slices were visualized under bright-field microscopy (Olympus BX51).

The scar elevation index (SEI) value was calculated according to H&E staining images as follows: SEI = H/H_0, where H refers to the height from the highest point to the cartilage surface of HSs, and H_0 is the height from the stratum corneum to the cartilage surface in adjacent normal skin. SEI was averaged from five HSs per group. And an SEI value higher than 1.5 was considered as scar formation.[35,36] Moreover, collagen volume fraction (CVF) was evaluated to assess the collagen deposition level in HSs. CVF was calculated as the ratio of collagen area to the total area of Masson's staining images. CVF was analyzed with five HSs for each treatment group.

2.5. Statistical analysis

All data are presented as mean value ± standard deviation. Cell experiments were conducted in triplicate three times. Animal studies were carried out using five rabbit HSs per group. One-way ANOVA was performed to evaluate the significant differences between different treatments using GraphPad Prism v. 6 (GraphPad Software, USA). And $P < 0.05$ was considered statistically significant.

3. Results

3.1. Effect of losartan on proliferation and migration of HSFs

Activated fibroblasts with abnormal proliferation and excessive migration lead to the overproduction of collagen in scars.[37] Consequently, the inhibition of proliferation and migration of HSFs is important in the treatment of HSs. First, the effect of losartan on the proliferation of human HSFs was investigated. Cell viability of HSFs was decreased after treatment with all concentrations of losartan (Fig. 2A). 1 μM losartan had a stronger inhibitory effect on the proliferation of HSFs than 10 and 100 μM losartan, but without significant difference (Fig. 2A). 1000 μM losartan showed the most significant inhibition effect on cell proliferation (Fig. 2A). However, considering severe cytotoxicity from high dosage, this concentration was not considered in subsequent experiments. The inhibitory effect of losartan on HSF proliferation was consistent with previous reports, where the proliferation of mouse fibroblasts was inhibited with treatment with an ACE inhibitor,[38] which worked on the same biochemical pathway as ARBs.

Subsequently, the migration of HSFs was evaluated with treatment of different concentrations of losartan. In the control group (0 μM losartan), the scratch underwent rapid healing due to the rapid migration of HSFs (Fig. 2B and C). In

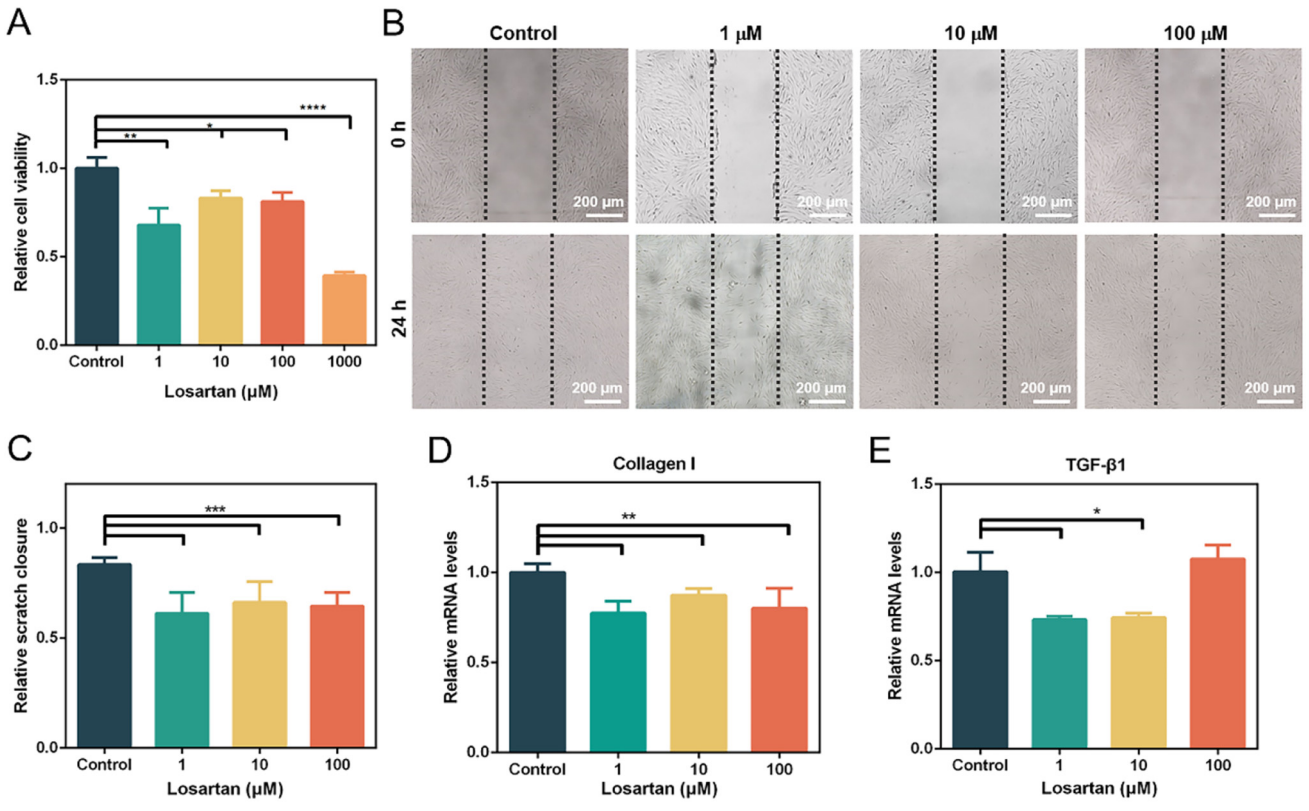

Fig. 2 Evaluation of impact of losartan on HSFs. (A) Viability of HSFs after treatment with different concentrations of losartan for 24 h. (B) Scratch-wound assay to evaluate the migration of HSFs treated with different concentrations of losartan. (C) Quantification of scratch wound closure after 24 h of treatment. (D and E) Relative mRNA expressions of TGF-β1 (D) and collagen I (E) in HSFs treated by different concentrations of losartan for 24 h. *$P < 0.05$; **$P < 0.01$; ***$P < 0.001$; ****$P < 0.0001$.

contrast, the migration of HSFs was significantly inhibited in losartan-treated groups (Fig. 2B and C), without significant difference in scratch closure among these groups (Fig. 2C). These results indicated that losartan effectively inhibited the migration of HSFs without concentration dependence. The inhibited migration of HSFs by losartan was consistent with the previous findings, where ARBs were associated with decreased migration and scar formation in a rat model.[39] Therefore, the treatment with losartan as an ARB effectively inhibited the proliferation and migration of HSFs, which has potential for prevention of HS formation.

3.2. Impact of losartan on gene expression associated with HS

Subsequently, the gene expression related to scar formation was investigated in HSFs after treatment with losartan. RNA expression of collagen I in HSFs was significantly down-regulated after treatment with 1, 10 and 100 μM losartan (Fig. 2D), indicating that losartan effectively inhibited the expression of collagen I in HSFs. TGF-β also plays a key role in the formation of scars.[40] The expression levels of TGF-β1 were significantly down-regulated with treatment with 1 μM and 10 μM losartan, but did not significantly vary with treatment of 100 μM losartan (Fig. 2E). The down-regulated TGF-β1 expression in HSFs was consistent with a previous observation in mice treated with an oral ACE inhibitor.[41] Moreover, TGF-β signaling may contribute to the activation of fibroblasts through TGF-β/Smad pathways.[40] Therefore the gene expression of Smad3 was also investigated. However, with treatment of different losartan concentrations, Smad3 expression levels of HSFs did not significantly change (Fig. S2A†). The ACE inhibitor restrained the phosphorylation of Smad2/3, while the total content of Smad2/3 was not affected,[41] which may explain the invariant expression levels of Smad3 (Fig. S2A†). In addition, the imbalance between pro-inflammatory and anti-inflammatory cytokines led to excessive collagen deposition in HSs.[40] IL-6, a proinflammatory factor, was overexpressed in HSs.[42] Here, the expression of IL-6 was significantly down-regulated under treatment with 10 μM losartan (Fig. S2B†). The suppression of IL-6 may help the healing of HSs.

3.3. Preparation and characterization of microneedle patches

Since HSs show great individual differences, herein, in order to meet the requirement of HSs with different shapes and thicknesses (Fig. 1A), we used stereolithographic 3D printing to fabricate personalized microneedle molds (Fig. S1†). By adjusting the 3D printing parameters, we designed and fabricated microneedle patches with personalized shapes and sizes (Fig. 1A). In this study, we used the square-shaped microneedle patch design for demonstration (Fig. 1A, right), each patch consisted of 11 × 11 needles, and each needle had a bottom diameter of 300 μm and a height of 800 μm, with a tip-to-tip space of 600 μm.

From the optical images, the fabricated microneedle patches with materials M1 and M2 showed a complete structure (Fig. S3A and B†), with a size of 7 mm × 7 mm of the substrate. However, the microneedle patches composed of material M3 showed significant deformation on the substrate (Fig. S3C†), due to the large shrinkage from the hydroxyapatite component during the drying process (Table 2).[13] The obtained microneedles exhibited a conical shape (Fig. 3A), with a bottom diameter of ~290 μm, a height of ~755 μm, and a tip-to-tip distance of ~592 μm (Fig. 3B and C). The final microneedle dimensions were slightly smaller than the above designed PDMS molds, mainly due to the shrinkage of gelatin and starch during the fabrication process (Fig. 1B).

3.4. Mechanical properties of microneedle patches

Since HS tissues exhibit stronger stiffness than normal skin, strong mechanical strength of microneedles is required for puncture into HSs. The mechanical properties of microneedle patches of materials M1 and M2 were assessed by the compression test; the microneedle patch of material M3 was not evaluated due to its poor shape morphology (Fig. S3†). With the increase of the compression displacement (Fig. 3D), the force between the probe and the microneedles increased continuously (Fig. 3E and F). When the force reached a certain degree, few microneedles broke, resulting in the sudden decrease of the force between the probe and the microneedle patch (Fig. 3F, black arrows). The further displacement of the probe continuously compressed the microneedle patch until all the microneedles were compressed, which led to a plateau region (Fig. 3E and F, red arrows) prior to the compaction stage of the substrate. Accordingly, the microneedle patches of materials M1 and M2 reached a failure force of 0.14 N per needle and 0.30 N per needle, respectively (Fig. 3F). The mechanical strength of these microneedles was strong enough for normal skin penetration[43–45] as well as for scar penetration.[20] The physical blending of gelatin and starch effectively improved the stability and mechanical strength of gelatin.[46] Compared to our previous study,[14] herein, the higher content of gelatin in the gelatin-starch blending (Table 2) resulted in the stronger mechanical property of the obtained microneedle patch (Fig. 3F). Accordingly, the microneedle patch of material M2 was selected for the next experiments due to its stronger mechanical strength.

3.5. Insertion capability and drug release of microneedle patches

First, we used porcine skin to evaluate the insertion capability of microneedles, since porcine skin has a similar structure to human skin but exhibits a higher yield stress than human skin,[20] which therefore can mimic the HS tissue to a certain degree. Microneedles of M1 and M2 can effectively penetrate the porcine skin, leaving visible channels on the porcine skin (Fig. S4A and B†). In contrast, the microneedles of material M3 were easily broken during the pressing process because of its irregular shape and brittleness (Fig. S3C†), therefore resulting in no visible changes on the porcine skin (Fig. S4C†). Microneedles loaded with rhodamine 6G were used for better visualization of microchannels formed in the porcine skin.

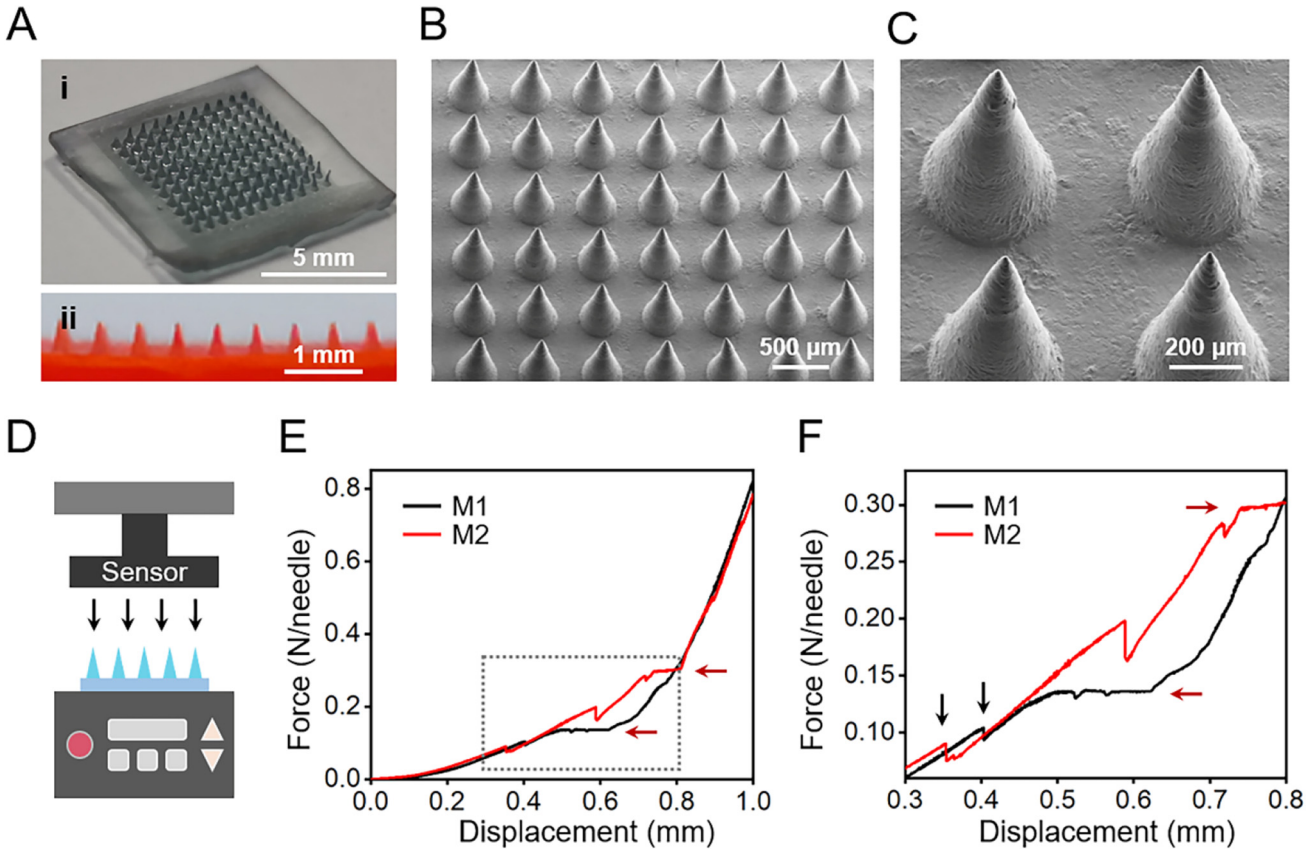

Fig. 3 Morphology and mechanical property of microneedle patches. (A) Optical images of microneedle patches, including vertical view of a patch (i), and cross-sectional view of a patch pre-loaded with rhodamine 6G (ii). (B and C) SEM images of microneedle patches with different magnifications. (D–F) Experimental setup (D) and mechanical performance (E and F) of microneedle patches prepared with different materials.

Fluorescence images revealed that the rhodamine 6G-loaded microneedle was evenly distributed in the cross section of the pierced porcine skin (Fig. 4A), with a deepest microchannel of 428.6 μm formed in the porcine skin (Fig. S5A†). These results revealed that the microneedles successfully penetrated the stratum corneum and reached the epidermis and dermis of the porcine skin. In addition, the *in vitro* drug release profile showed that the loaded drugs in microneedles were burst released upon the rapid dissolution of gelatin and starch in solution (Fig. S5B†). Comparably, the drug release of microneedles in skin tissues would be slowed down, due to the limited interstitial fluid in the skin. After insertion of the microneedles into porcine skin for 10 min, the fluorescence of rhodamine 6G can be detected in the skin tissue around the microchannels formed by microneedles, suggesting that the released drugs successfully permeated into the porcine skin (Fig. S5A†).

Further, we investigated the penetration ability of losartan-loaded microneedles into HSs on rabbit ear. After insertion and removal of the losartan-loaded microneedle patches, visible channels were formed in the rabbit HSs, with minimal bleeding observed on the surface of rabbit HSs (Fig. 4B and Fig. S6A–D†). H&E staining images also confirmed that the losartan-loaded microneedles successfully penetrated the stratum corneum of HSs (Fig. 4C and Fig. S6E–H†). These results demonstrated that the losartan-loaded microneedles can successfully puncture the stratum corneum of HSs, which is beneficial for effective intradermal delivery of drugs into HSs for treatment.

3.6. Dissolution of losartan-loaded microneedles

Favorable dissolution of microneedle materials is essential for efficient drug delivery and therapeutics into the skin or into HSs.[14,15] The optimized microneedles of material M2 were composed of gelatin and starch (Table 2). Gelatin is a protein with water-solubility and biodegradability, and the degradation product can be absorbed *in vivo*.[47] Starch is also a biodegradable polymer widely involved in the food and drug industry.[48] After insertion of losartan-loaded microneedles into HSs, almost all the needle parts of the patches were dissolved (Fig. S7†). SEM images also confirmed that nearly all the main block of needles was dissolved compared to those needles before insertion into HSs (Fig. 4D and E). The above results revealed that losartan-loaded microneedles can dissolve within a short period of time, and their dissolution and absorption *in vivo* is beneficial for losartan delivery into HSs for further therapeutic effect.

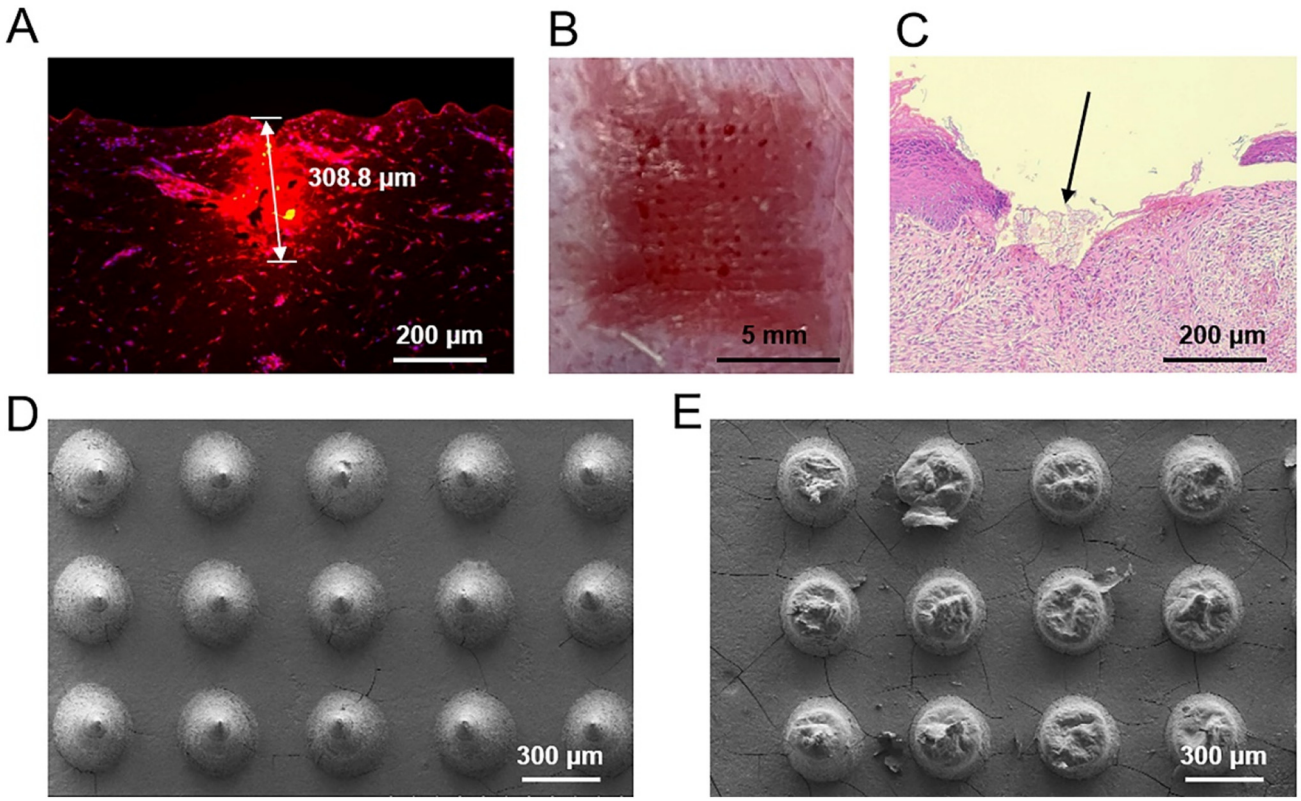

Fig. 4 Effect of penetration of microneedle patches. (A) Confocal image of porcine skin after insertion with a rhodamine 6G-loaded microneedle patch. (B) Image of rabbit HS after insertion with an LMN-4 patch. (C) H&E staining image of rabbit HS after insertion with an LMN-4 patch. The black arrow indicates the broken stratum corneum of the scar. (D and E) SEM images of microneedles before (D) and after (E) insertion into rabbit HS.

3.7. Treatment effect of losartan-loaded microneedles on rabbit HSs

Prior to investigating the treatment effect of losartan-loaded microneedles on rabbit HSs, the concentration of losartan in microneedles was optimized. Microneedle patches loaded with different concentrations of losartan (Table 3) were used to treat HSs in rabbit ears. After three administration, H&E staining images of HSs showed that a small amount of bleeding existed inside the dermis of HSs treated with LMN-1 and LMN-2 groups (Fig. S8A and B,† yellow arrows). In contrast, no bleeding was observed in the sections of HSs after LMN-3 and LMN-4 treatments (Fig. S8C and D†). Comparably, LMN-4 treatment reduced the HSs more effectively than LMN-3 treatment (Fig. S8C and D†). Combining the comprehensive treatment effect (Fig. S8†) and the lower toxicity from lower drug dosage (Table 3), LMN-4 was selected for the next therapeutic experiment.

The treatment effect of HSs in rabbit ears was further investigated using different treatment groups, including control without any treatment, drug-free MN, LMN-4, losartan cream, and Mepiform, respectively. Mepiform is a commercialized self-adherent soft silicone dressing for care and management of scars, and served as a negative control.[5] After three administration, HSs in the control group showed significantly elevated tubercular scars with dark color (Fig. 5). HSs treated with the drug-free MN group also showed dark-red color and protruded surface (Fig. 5). Comparably, HSs treated with the LMN-4 group were smooth, and the color was much closer to adjacent normal skin (Fig. 5). The application of losartan cream did not effectively reduce the dark color of HSs, and the HSs showed dark protrusion in the center (Fig. 5). Mepiform treatment effectively reduced the dark color and protrusion of HSs compared to the control group; however, Mepiform-treated HSs showed a darker color and severer protrusion than the LMN-4 treatment group.

H&E staining was performed to evaluate the histological changes in HSs, and SEI value was quantified to evaluate the degree of dermal hypertrophy in HSs. In the control group, hyperplasia existed in the epidermis and dermis in HSs, with a much larger number of fibroblasts in HSs (Fig. 6A and B), and the SEI of the control group was significantly elevated (Fig. 7A). HSs treated with the drug-free MN group showed similar histological manifestation to the control group, with neutrophil infiltration existing in both groups (Fig. 6A and B). The SEI value of the drug-free MN group was as high as the control group (Fig. 7A). Compared with the control and drug-free MN group, LMN-4 treatment significantly decreased the

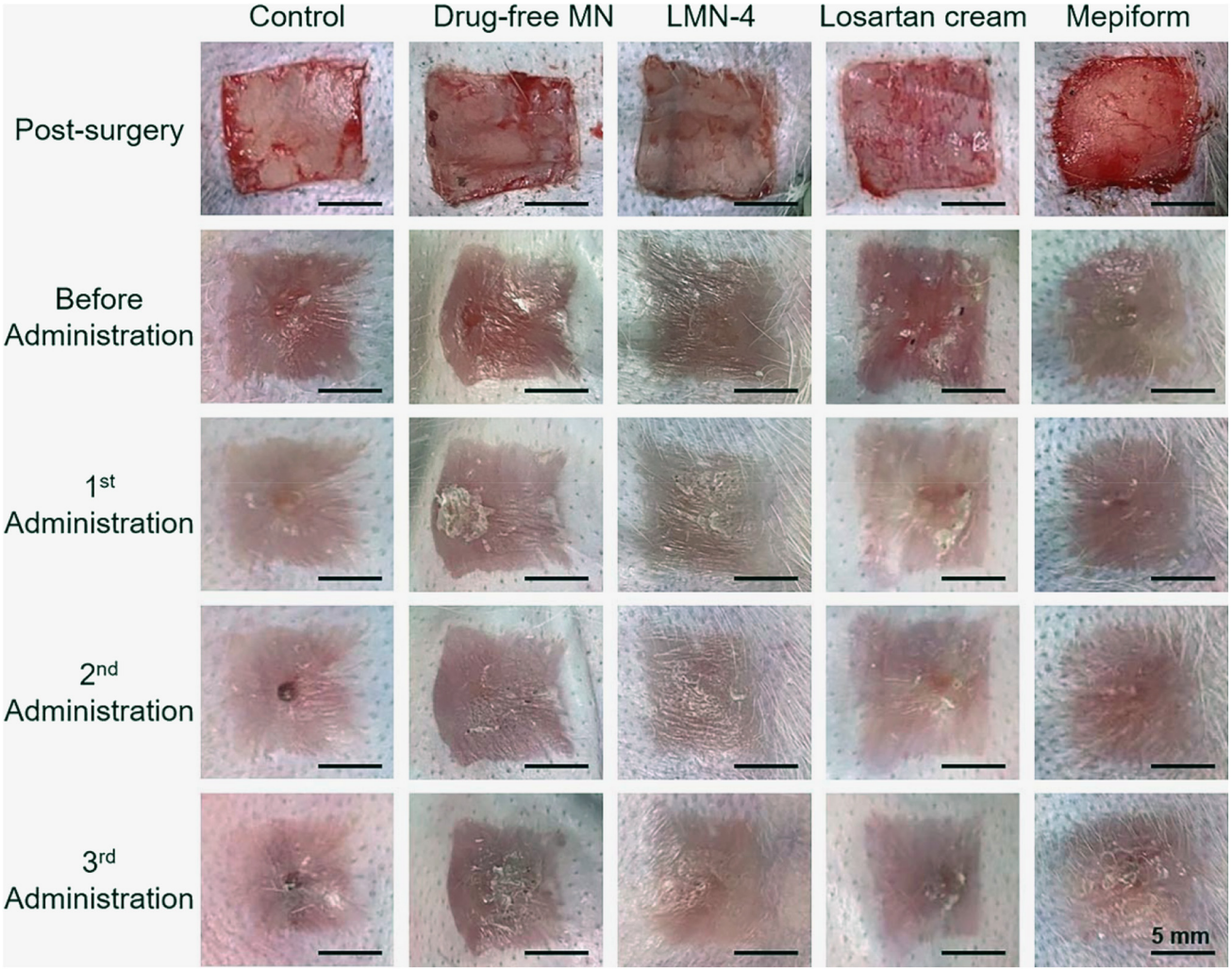

Fig. 5 Treatment effect on rabbit HSs by different groups.

SEI of HSs (Fig. 7A), with less dense fibroblasts in HSs than other treatment groups (Fig. 6A and B). Losartan cream and Mepiform treatments slightly decreased the SEI value of HSs compared to the control group (Fig. 7A), and dense fibroblasts still existed in these treatment groups (Fig. 6A and B).

In addition, Masson's trichrome staining was conducted to assess the deposition of collagen fibers in HS tissues, since excessive deposition of collagen is a vital characteristic of HS formation.[2] For control and drug-free MN groups, dense, curly and disordered collagen fibers were accumulated in HS tissues (Fig. 6C, blue color). Compared to the control group, the collagen fibers in HSs treated with the LMN-4 group were wispy and sparse, and arranged more regularly in almost the same direction (Fig. 6C). In contrast, for losartan cream and Mepiform treatment, HSs showed large amounts of collagen fibers, and the arrangement of collagen fibers remained irregular (Fig. 6C). The quantitative measurement of the collagen area also revealed that LMN-4 treatment can effectively reduce the deposition of collagen in HSs (Fig. 7B).

4. Discussion

Herein, we successfully designed and fabricated a personalized microneedle patch for effective intradermal losartan delivery and therapy of rabbit HSs. The microneedle patches were personalized designed according to individual HS with different shapes and thicknesses (Fig. 1A), and stereolithographic 3D printing was employed to print the personalized molds with different geometric design (Fig. S1†),[49] and then the template molding method was used to prepare the losartan-loaded dissolving microneedle patches (Fig. 1B). Dissolving microneedle patches composed of gelatin and starch were selected for intradermal drug delivery, where the drugs loaded in the microneedles can be released into the HS tissues upon the dissolution of microneedles.[20] The physical blending of gelatin and starch is effective to improve the stability and mechanical strength of gelatin.[46] Based on our previous work where the gelatin–starch mixture was used to prepare microneedles,[14] herein, either gelatin content in the mixture was increased or inorganic

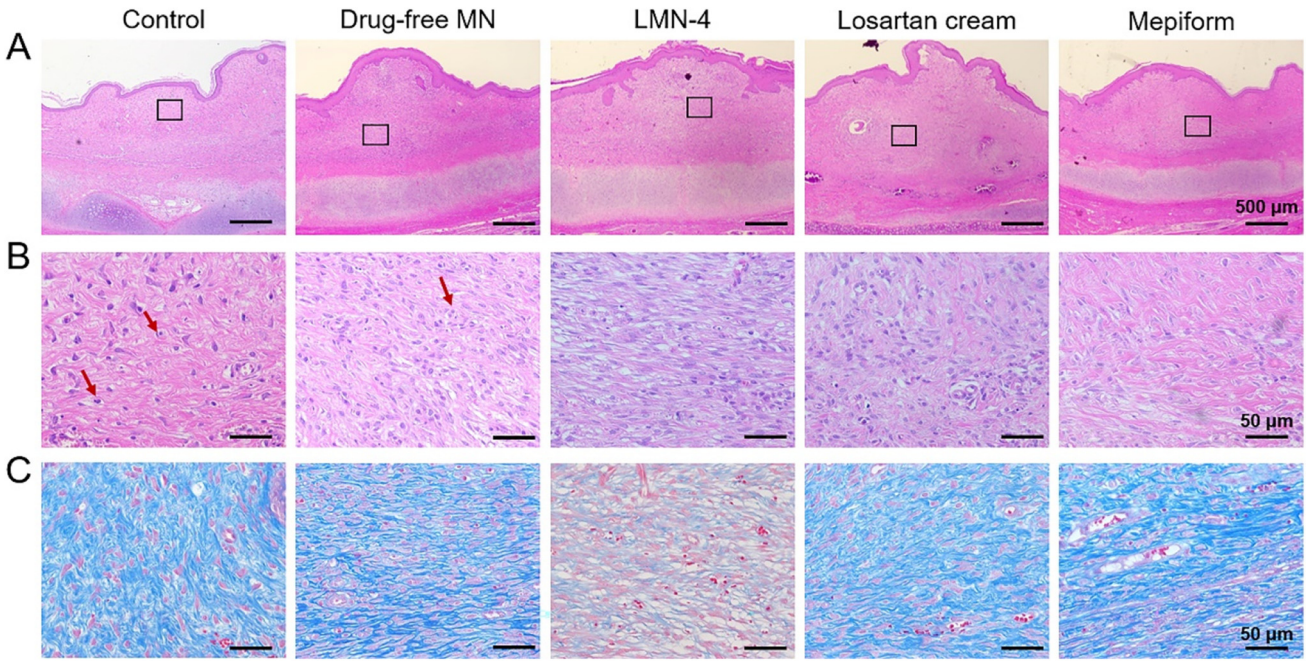

Fig. 6 Histological analysis of HSs with different treatments. (A) Representative H&E staining images of rabbit HSs after different treatments. (B) Magnified H&E staining images corresponding to the regions in (A). The red arrows indicate the neutrophil infiltration. (C) Masson's staining images of rabbit HSs after different treatments.

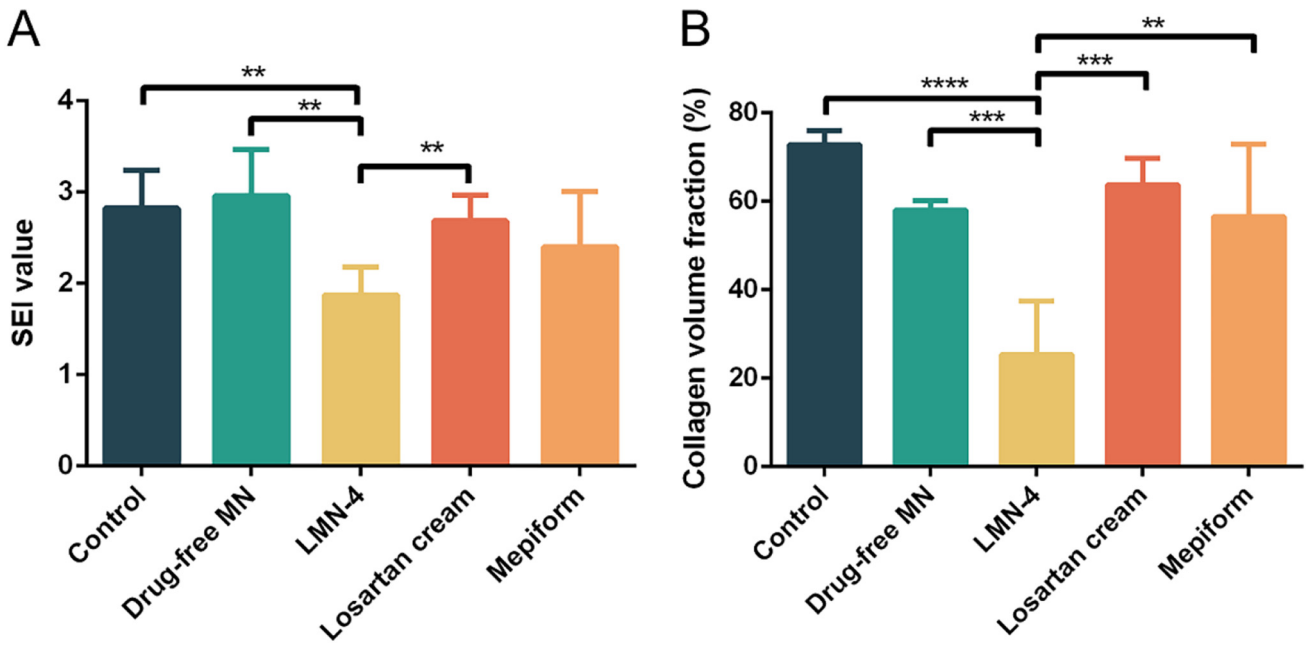

Fig. 7 (A) SEI and (B) CVF of HSs after different treatments. $^{**}P < 0.01$; $^{***}P < 0.001$; $^{****}P < 0.0001$.

materials were added into the mixture (Table 2), in order to further increase the mechanical strength of the microneedles, with the aim to facilitate their penetration into more rigid HS tissues. However, the addition of hydroxyapatite into microneedles[13,50] led to significant deformation of the composite patch (Fig. S3†). In contrast, the increase of gelatin content in the gelatin–starch mixture led to a stronger mechanical strength of the microneedles with a good morphology (Fig. 3 and Fig. S3†). The optimized microneedles of material M2 exhibited a sharp and conical structure (Fig. 3A–C), and can effectively penetrate the thick and rigid porcine skin (Fig. S4 and S5†) as well as the HSs in rabbit ears (Fig. 4 and Fig. S6†).

Losartan belongs to a drug class of ARBs, which can reduce blood pressure by helping blood vessels to relax and is widely used in end-organ protection.[51] Recently, losartan was also reported for treatment of scars. For example, oral administration of ARBs was adopted for scar prevention and treatment,[41] and topical use of losartan cream effectively inhibited scar formation,[52] with inhibited formation of blood vessels and increased flexibility of scars.[53] However, oral administration of ARBs for treatment of HSs may have side effects such as hypotension, angioedema, and so on.[52] Losartan cream may avoid the side effects of oral medication, but the thick stratum corneum and the dense collagen fibers of HSs limit the efficiency of drug penetration.[52] Herein, the dissolving microneedle array patch as a carrier of losartan was employed, in order to improve the drug delivery efficiency directly into the dermis of HSs. After penetration into HS tissues and upon the dissolution of the microneedles (Fig. S7† and Fig. 4E), the losartan loaded in the microneedles was released into HSs for therapeutic effect. The released losartan into HS tissues inhibited the proliferation and migration of HSFs (Fig. 2A–C), and decreased the gene expression of TGF-β1 (Fig. 2E), inflammatory factors such as IL-6 (Fig. S2B†), and collagen I in HSFs (Fig. 2D). Together, losartan-loaded microneedles effectively inhibited the HS formation in rabbit ears (Fig. 5), with a decreased SEI value (Fig. 6), and with less fibrosis deposition and collagen deposition in the HSs (Fig. 7).

Together, we successfully designed a personalized dissolving microneedle patch system, and demonstrated its intradermal delivery of losartan into HSs for effective treatment of rabbit HSs. This personalized microneedle patch system opens a new window for management and treatment of skin diseases such as HSs, keloid, closed wounds, cutaneous melanoma, and so on. In the future, flexible microneedles[18,54] can be designed for better adhesion to HS tissues. Moreover, a combined strategy, such as Mepiform® soft silicone sheeting for physical treatment dressing and drug-loaded microneedles for scar treatment, can be used for improved performance in scar management.

5. Conclusions

In this study, we successfully prepared a personalized dissolving microneedle patch system, for transdermal delivery of losartan and effective treatment of HSs in a rabbit ear model. The optimized microneedles composed of gelatin and starch exhibited strong mechanical strength, and effectively penetrated the stratum corneum of HSs, and therefore increased the intradermal delivery of losartan into HSs upon the dissolution of microneedles. Losartan effectively inhibited the proliferation and migration of HSFs, and inhibited scar hyperplasia by down-regulating the gene expression of TGF-β1, IL-6 and collagen I. Together, the personalized losartan-loaded microneedles effectively decreased the formation of HSs in rabbit ears, with a reduced SEI value, more regular tissue arrangement, and decreased deposition of collagen in HSs. This personalized microneedle patch system improved the compliance of patients, and increased the efficiency of drug delivery into HSs, which has good application prospect in personalized treatment of skin diseases.

Conflicts of interest

There are no conflicts of interest to declare.

Acknowledgements

The work was supported by the National Natural Science Foundation of China (NSFC, grant number: 81871484 and 82172096) and Zhongnan Hospital Science and Technology Innovation Cultivation Foundation (grant number: CXPY2020039).

References

1 J. Q. Coentro, E. Pugliese, G. Hanley, M. Raghunath and D. I. Zeugolis, Current and upcoming therapies to modulate skin scarring and fibrosis, *Adv. Drug Delivery Rev.*, 2019, **146**, 37–59.
2 Z. C. Wang, W. Y. Zhao, Y. Cao, Y. Q. Liu, Q. Sun, P. Shi, J. Q. Cai, X. Z. Shen and W. Q. Tan, The roles of inflammation in keloid and hypertrophic scars, *Front. Immunol.*, 2020, **11**, 603187.
3 H. J. Lee and Y. J. Jang, Recent understandings of biology, prophylaxis and treatment strategies for hypertrophic scars and keloids, *Int. J. Mol. Sci.*, 2018, **19**, 711.
4 G. G. Gauglitz, H. C. Korting, T. Pavicic, T. Ruzicka and M. G. Jeschke, Hypertrophic scarring and keloids: pathomechanisms and current and emerging treatment strategies, *Mol. Med.*, 2011, **17**, 113–125.
5 K. C. Hsu, C. W. Luan and Y. W. Tsai, Review of silicone gel sheeting and silicone gel for the prevention of hypertrophic scars and keloids, *Wounds*, 2017, **29**, 154–158.
6 P. Singh, A. Carrier, Y. Chen, S. Lin, J. Wang, S. Cui and X. Zhang, Polymeric microneedles for controlled transdermal drug delivery, *J. Controlled Release*, 2019, **315**, 97–113.
7 X. Zhang, Y. Wang, J. Chi and Y. Zhao, Smart microneedles for therapy and diagnosis, *Research*, 2020, **2020**, 7462915.
8 X. P. Zhang, Y. T. He, W. X. Li, B. Z. Chen, C. Y. Zhang, Y. Cui and X. D. Guo, An update on biomaterials as microneedle matrixes for biomedical applications, *J. Mater. Chem. B*, 2022, **10**, 6059–6077.
9 X. Sun, W. Ji, B. Zhang, L. Ma, W. Fu, W. Qian, X. Zhang, J. Li, E. Sheng, Y. Tao and D. Zhu, A theranostic microneedle array patch for integrated glycemia sensing and self-regulated release of insulin, *Biomater. Sci.*, 2022, **10**, 1209–1216.
10 Y. Wang, H. Liu, X. Yang, Z. Shi, J. Li, L. Xue, S. Liu and Y. Lei, A responsive hydrogel-based microneedle system for

minimally invasive glucose monitoring, *Smart Mater. Med.*, 2023, **4**, 69–77.

11 X. Jiang and P. B. Lillehoj, Microneedle-based skin patch for blood-free rapid diagnostic testing, *Microsyst. Nanoeng.*, 2020, **6**, 96.

12 Y. Zhang, J. Li, M. Wu, Z. Guo, D. Tan, X. Zhou, Y. Li, S. Liu, L. Xue and Y. Lei, Glucose-responsive gold nanocluster-loaded microneedle patch for type 1 diabetes therapy, *ACS Appl. Bio Mater.*, 2020, **3**, 8640–8649.

13 M. Wu, Y. Zhang, H. Huang, J. Li, H. Liu, Z. Guo, L. Xue, S. Liu and Y. Lei, Assisted 3D printing of microneedle patches for minimally invasive glucose control in diabetes, *Mater. Sci. Eng., C*, 2020, **117**, 111299.

14 Y. Zhang, M. Wu, D. Tan, Q. Liu, R. Xia, M. Chen, Y. Liu, L. Xue and Y. Lei, A dissolving and glucose-responsive insulin-releasing microneedle patch for type 1 diabetes therapy, *J. Mater. Chem. B*, 2021, **9**, 648–657.

15 H. T. T. Duong, Y. Yin, T. Thambi, B. S. Kim, J. H. Jeong and D. S. Lee, Highly potent intradermal vaccination by an array of dissolving microneedle polypeptide cocktails for cancer immunotherapy, *J. Mater. Chem. B*, 2020, **8**, 1171–1181.

16 H. Amani, M.-A. Shahbazi, C. D'Amico, F. Fontana, S. Abbaszadeh and H. A. Santos, Microneedles for painless transdermal immunotherapeutic applications, *J. Controlled Release*, 2021, **330**, 185–217.

17 J. Chi, X. Zhang, C. Chen, C. Shao, Y. Zhao and Y. Wang, Antibacterial and angiogenic chitosan microneedle array patch for promoting wound healing, *Bioact. Mater.*, 2020, **5**, 253–259.

18 Z. Zeng, G. Jiang, Y. Sun, U. E. Aharodnikau, K. E. Yunusov, X. Gao, T. Liu and S. O. Solomevich, Rational design of flexible microneedles coupled with CaO2@PDA-loaded nanofiber films for skin wound healing on diabetic rats, *Biomater. Sci.*, 2022, **10**, 5326–5339.

19 Z. Guo, H. Liu, Z. Shi, L. Lin, Y. Li, M. Wang, G. Pan, Y. Lei and L. Xue, Responsive hydrogel-based microneedle dressing for diabetic wound healing, *J. Mater. Chem. B*, 2022, **10**, 3501–3511.

20 Y. Xie, H. Wang, J. Mao, Y. Li, M. Hussain, J. Zhu, Y. Li, L. Zhang, J. Tao and J. Zhu, Enhanced in vitro efficacy for inhibiting hypertrophic scar by bleomycin-loaded dissolving hyaluronic acid microneedles, *J. Mater. Chem. B*, 2019, **7**, 6604–6611.

21 S. Lin, G. Quan, A. Hou, P. Yang, T. Peng, Y. Gu, W. Qin, R. Liu, X. Ma, X. Pan, H. Liu, L. Wang and C. Wu, Strategy for hypertrophic scar therapy: improved delivery of triamcinolone acetonide using mechanically robust tip-concentrated dissolving microneedle array, *J. Controlled Release*, 2019, **306**, 69–82.

22 Y. Y. Chun, W. W. R. Tan, M. I. G. Vos, W. K. Chan, H. L. Tey, N. S. Tan and T. T. Y. Tan, Scar prevention through topical delivery of gelatin-tyramine-siSPARC nanoplex loaded in dissolvable hyaluronic acid microneedle patch across skin barrier, *Biomater. Sci.*, 2022, **10**, 3963–3971.

23 H. Du, P. Liu, J. Zhu, J. Lan, Y. Li, L. Zhang, J. Zhu and J. Tao, Hyaluronic acid-based dissolving microneedle patch loaded with methotrexate for improved treatment of psoriasis, *ACS Appl. Mater. Interfaces*, 2019, **11**, 43588–43598.

24 M. R. Prausnitz and R. Langer, Transdermal drug delivery, *Nat. Biotechnol.*, 2008, **26**, 1261–1268.

25 J. Poetschke and G. G. Gauglitz, Current options for the treatment of pathological scarring, *J. Dtsch. Dermatol. Ges.*, 2016, **14**, 467–477.

26 R. Ogawa, The most current algorithms for the treatment and prevention of hypertrophic scars and keloids: a 2020 update of the algorithms published 10 years ago, *Plast. Reconstr. Surg.*, 2022, **149**, 79e–94e.

27 K. Hedayatyanfard, N. S. Haddadi, S. A. Ziai, H. Karim, F. Niazi, U. M. Steckelings, B. Habibi, A. Modarressi and A. R. Dehpour, The renin-angiotensin system in cutaneous hypertrophic scar and keloid formation, *Exp. Dermatol.*, 2020, **29**, 902–909.

28 U. M. Steckelings, T. Wollschlager, J. Peters, B. M. Henz, B. Hermes and M. Artuc, Human skin: source of and target organ for angiotensin II, *Exp. Dermatol.*, 2004, **13**, 148–154.

29 K. Morihara, S. Takai, H. Takenaka, M. Sakaguchi, Y. Okamoto, T. Morihara, M. Miyazaki and S. Kishimoto, Cutaneous tissue angiotensin-converting enzyme may participate in pathologic scar formation in human skin, *J. Am. Acad. Dermatol.*, 2006, **54**, 251–257.

30 T. Ehanire, L. Ren, J. Bond, M. Medina, G. Li, L. Bashirov, L. Chen, G. Kokosis, M. Ibrahim, A. Selim, G. C. Blobe and H. Levinson, Angiotensin II stimulates canonical TGF-beta signaling pathway through angiotensin type 1 receptor to induce granulation tissue contraction, *J. Mol. Med.*, 2015, **93**, 289–302.

31 M. Sato, R. M. Engelman, H. Otani, N. Maulik, J. A. Rousou, J. E. Flack 3rd, D. W. Deaton and D. K. Das, Myocardial protection by preconditioning of heart with losartan, an angiotensin II type 1-receptor blocker: implication of bradykinin-dependent and bradykinin-independent mechanisms, *Circulation*, 2000, **102**, III346–III351.

32 X. Zhou, Y. Xie, H. Xiao, X. Deng, Y. Wang, L. Jiang, C. Liu and R. Zhou, MicroRNA-519d inhibits proliferation and induces apoptosis of human hypertrophic scar fibroblasts through targeting Sirtuin 7, *Biomed. Pharmacother.*, 2018, **100**, 184–190.

33 D. E. Morris, L. Wu, L. L. Zhao, L. Bolton, S. I. Roth, D. A. Ladin and T. A. Mustoe, Acute and chronic animal models for excessive dermal scarring: quantitative studies, *Plast. Reconstr. Surg.*, 1997, **100**, 674–681.

34 O. Kloeters, A. Tandara and T. A. Mustoe, Hypertrophic scar model in the rabbit ear: a reproducible model for studying scar tissue behavior with new observations on silicone gel sheeting for scar reduction, *Wound Repair Regen.*, 2007, **15**, S40–S45.

35 B. Yang, Y. Dong, Y. Shen, A. Hou, G. Quan, X. Pan and C. Wu, Bilayer dissolving microneedle array containing 5-fluorouracil and triamcinolone with biphasic release

profile for hypertrophic scar therapy, *Bioact. Mater.*, 2021, **6**, 2400–2411.

36 Z. Yu, X. Meng, S. Zhang, X. Wang, Y. Chen, P. Min, Z. Zhang and Y. Zhang, IR-808 loaded nanoethosomes for aggregation-enhanced synergistic transdermal photodynamic/photothermal treatment of hypertrophic scars, *Biomater. Sci.*, 2022, **10**, 158–166.

37 M. Pikula, M. E. Zebrowska, L. Poblocka-Olech, M. Krauze-Baranowska, M. Sznitowska and P. Trzonkowski, Effect of enoxaparin and onion extract on human skin fibroblast cell line - therapeutic implications for the treatment of keloids, *Pharm. Biol.*, 2014, **52**, 262–267.

38 Q. Q. Fang, X. F. Wang, W. Y. Zhao, S. L. Ding, B. H. Shi, Y. Xia, H. Yang, L. H. Wu, C. Y. Li and W. Q. Tan, Angiotensin-converting enzyme inhibitor reduces scar formation by inhibiting both canonical and noncanonical TGF-beta1 pathways, *Sci. Rep.*, 2018, **8**, 3332.

39 A. Murphy, T. LeVatte, C. Boudreau, C. Midgen, P. Gratzer, J. Marshall and M. Bezuhly, Angiotensin II type I receptor blockade is associated with decreased cutaneous scar formation in a rat model, *Plast. Reconstr. Surg.*, 2019, **144**, 803e–813e.

40 B. Berman, A. Maderal and B. Raphael, Keloids and hypertrophic scars: pathophysiology, classification, and treatment, *Dermatol. Surg.*, 2017, **43**, S3–S18.

41 W. Q. Tan, Q. Q. Fang, X. Z. Shen, J. F. Giani, T. V. Zhao, P. Shi, L. Y. Zhang, Z. Khan, Y. Li, L. Li, J. H. Xu, E. A. Bernstein and K. E. Bernstein, Angiotensin-converting enzyme inhibitor works as a scar formation inhibitor by down-regulating Smad and TGF-beta-activated kinase 1 (TAK1) pathways in mice, *Br. J. Pharmacol.*, 2018, **175**, 4239–4252.

42 D. Zhang, B. Li and M. Zhao, Therapeutic strategies by regulating interleukin family to suppress inflammation in hypertrophic scar and keloid, *Front. Pharmacol.*, 2021, **12**, 667763.

43 S. P. Davis, B. J. Landis, Z. H. Adams, M. G. Allen and M. R. Prausnitz, Insertion of microneedles into skin: measurement and prediction of insertion force and needle fracture force, *J. Biomech.*, 2004, **37**, 1155–1163.

44 W. Li, R. N. Terry, J. Tang, M. R. Feng, S. P. Schwendeman and M. R. Prausnitz, Rapidly separable microneedle patch for the sustained release of a contraceptive, *Nat. Biomed. Eng.*, 2019, **3**, 220–229.

45 B. Z. Chen, L. Q. Zhang, Y. Y. Xia, X. P. Zhang and X. D. Guo, A basal-bolus insulin regimen integrated microneedle patch for intraday postprandial glucose control, *Sci. Adv.*, 2020, **6**, eaba7260.

46 N. Z. Zhang, H. S. Liu, L. Yu, X. X. Liu, L. Zhang, L. Chen and R. Shanks, Developing gelatin-starch blends for use as capsule materials, *Carbohydr. Polym.*, 2013, **92**, 455–461.

47 S. Young, M. Wong, Y. Tabata and A. G. Mikos, Gelatin as a delivery vehicle for the controlled release of bioactive molecules, *J. Controlled Release*, 2005, **109**, 256–274.

48 C. Elvira, J. F. Mano, J. San Román and R. L. Reis, Starch-based biodegradable hydrogels with potential biomedical applications as drug delivery systems, *Biomaterials*, 2002, **23**, 1955–1966.

49 C. Y. Liaw and M. Guvendiren, Current and emerging applications of 3D printing in medicine, *Biofabrication*, 2017, **9**, 024102.

50 W. Chen, R. Tian, C. Xu, B. C. Yung, G. Wang, Y. Liu, Q. Ni, F. Zhang, Z. Zhou, J. Wang, G. Niu, Y. Ma, L. Fu and X. Chen, Microneedle-array patches loaded with dual mineralized protein/peptide particles for type 2 diabetes therapy, *Nat. Commun.*, 2017, **8**, 1777.

51 D. A. Sica, T. W. Gehr and S. Ghosh, Clinical pharmacokinetics of losartan, *Clin. Pharmacokinet.*, 2005, **44**, 797–814.

52 B. Zheng, Q. Q. Fang, X. F. Wang, B. H. Shi, W. Y. Zhao, C. Y. Chen, M. X. Zhang, L. Y. Zhang, Y. Y. Hu, P. Shi, L. Ma and W. Q. Tan, The effect of topical ramipril and losartan cream in inhibiting scar formation, *Biomed. Pharmacother.*, 2019, **118**, 109394.

53 K. Hedayatyanfard, S. A. Ziai, F. Niazi, I. Habibi, B. Habibi and H. Moravvej, Losartan ointment relieves hypertrophic scars and keloid: a pilot study, *Wound Repair Regen.*, 2018, **26**, 340–343.

54 I. Woodhouse, S. Nejati, V. Selvamani, H. Jiang, S. Chittiboyina, J. Grant, Z. Mutlu, J. Waimin, N. S. Abutaleb, M. N. Seleem and R. Rahimi, Flexible microneedle array patch for chronic wound oxygenation and biofilm eradication, *ACS Appl. Bio Mater.*, 2021, **4**, 5405–5415.